Geosciences and Engineering, Vol. 9, No. 14 (2021), pp. 96–115.
https://doi.org/10.33030/geosciences.2021.14.096

INVESTIGATION OF GAS FLOW MODELS IN CASE OF MICRO- AND NANOPORE SIZE RESERVOIRS

PATRIK PUSZTAI[1, *] – ANITA JOBBIK[1]

[1]*Research Institute of Applied Earth Sciences, University of Miskolc*
[*]*patrpusztai@mol.hu*

Abstract: Conventional continuum-flow equations, such as the well-known Darcy's law, greatly underestimate the fluid-flow rate when applied to micro and nanopore-bearing reservoirs. This paper concentrates on the collection, interpretation and presentation of different flow models which can be used in such conditions. They are utilized on core samples which originated in a Hungarian reservoir under extreme pressure and temperature (over 1,100 bar and 200 °C). As only limited literature is available which can describe the exact flow behavior of natural gas in these conditions, comparison of the different models under these conditions can provide information for a wider understanding of these types of reservoirs.

Several factors influence gas production from these unconventional formations, so the creation of an adequate material balance equation was necessary to describe pressure depletion and original gas in-place. Integration of this novel material balance equation with the different flow models results in a calculation algorithm which enables investigation of the reservoir behavior during production. Finally, the adaptability of this model to real production data is investigated.

Keywords: *fluid flow, nanopore, natural gas, material balance*

1. INTRODUCTION

The growing requirement for energy and the decreasing quantity of fossil fuels areforcing engineers to find alternative solutions. This phenomenon is valid in the case of hydrocarbons too, where the role of unconventional reservoirs is becoming more significant. Natural gas production from these types of reservoirs has been developed remarkably in the past few decades thanks to technological advancement.

These types of reservoirs (tight gas, shale gas) usually have a pore size distribution in the range of micro- to nanometers and the reservoirs are placed in extreme conditions, which influence the equations describing the gas flow and the material balance equations. Appropriate description and modeling of these mechanisms are indispensable for economic exploitation of unconventional natural gas reservoirs.

2. MATERIAL BALANCE EQUATION

Investigation of the multiple mechanisms which characterize the tight and shale gas reservoirs is necessary. Shale gas reservoirs are organic-rich, fine-grained reservoirs in which the pore space can be classified into three main categories: porous in

organic matter, interparticle pore system in the organic matrix, and open fractures (induced by hydraulic fracture stimulation and natural fractures). Natural gas (mainly methane) in shale gas reservoirs is generally believed to be stored as either free or adsorbed gas, although solution gas within pore fluids and bitumen may also be important [1]. There are multiple mechanisms for gas storage in organic-rich shales including [2]:

1. Adsorption upon internal surface area;
2. Conventional (compressed gas) storage in natural and hydraulic (induced) fractures;
3. Conventional storage in matrix porosity (organic and inorganic);
4. Solution in formation water;
5. Absorption (solution) in organic matter.

This paper concentrates on the 1st, 3rd and 4th mechanisms, as later the investigated formation is not considered to be fractured and the effect of absorption is neglected in this study. The total organic content (TOC) has a near linear relationship with the total gas content of shale reservoirs [3].

In the following two subsection the explanation of the 1st and 4th mechanisms are detailed, as they can be investigated in different ways.

2.1. Adsorption

The matrix systems of shale reservoirs (also coalbed methane – CBM) have immense capacity for methane storage. The mechanism by which this occurs is called adsorption. In adsorption, molecules of gas become attached to the surface of coal or to organic material in shale (which is obviously proportional to the total carbon content of the formation). Nearly all of the gas stored by adsorption to shale exists in a condensed, near liquid state. In order to simulate gas production in shale gas reservoirs, an accurate model of gas adsorption is very important. There are two different types of adsorption: chemical adsorption and physical adsorption. This paper deals with only physical adsorption as it is more relevant in reservoir engineering.

The expression of adsorption isotherm must be introduced, as the temperatures of reservoirs are assumed to be constant in this paper. It is assumed that at a given temperature the volume of adsorbed gas is only pressure dependent in the case of a given gas component and a given adsorbent [4].

This paper suggests the use of the so-called Langmuir isotherm, which is one of the most commonly applied adsorption models for shale gas reservoirs. It is based on the assumption that there is a dynamic equilibrium at constant temperature and pressure between adsorbed and non-adsorbed gas. Also, it is assumed that there is only a single layer of molecules covering the solid surface. The Langmuir isotherm has two fitting parameters: Langmuir volume (V_L) and Langmuir pressure (P_L). The typical formulation of a Langmuir isotherm is shown in *Equation (1)*, where V is the adsorbed gas volume at pressure p, V_L is the Langmuir volume or the maximum

gas volume of adsorption at infinite pressure, and P_L is the Langmuir pressure, which is the pressure corresponding to one-half Langmuir volume [5].

$$V = \frac{V_L \times p}{P_L + p} \tag{1}$$

In *Equation (1)* the V_L [sm^3/ton] and P_L [bar] values are determined in laboratory tests and their values are proportional to temperature, adsorbent material, and adsorbed material. *Figure 1* shows the Langmuir isotherm of the investigated reservoir in this paper (detailed later).

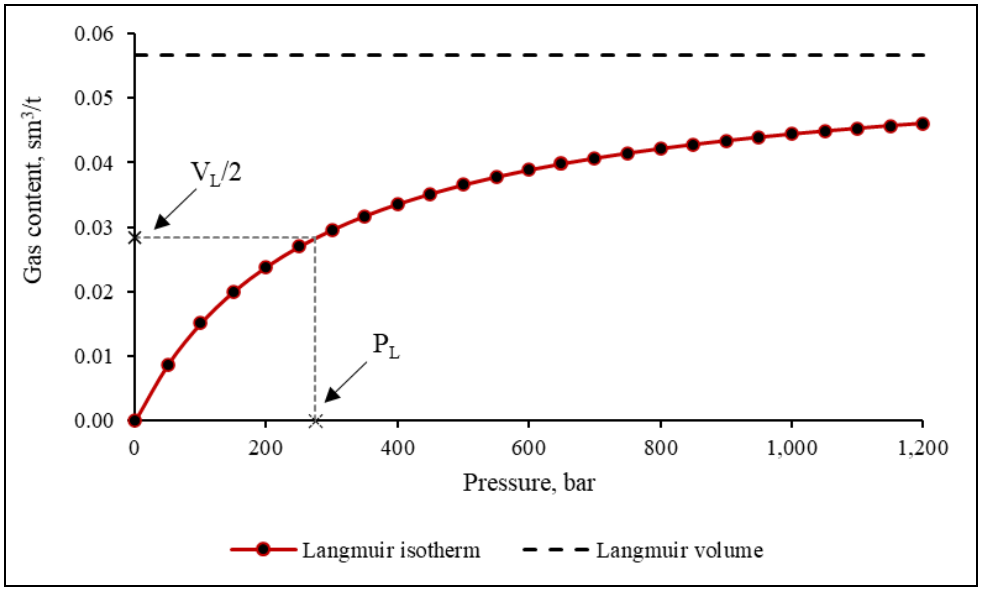

Figure 1
Langmuir isotherm of the investigated reservoir at P_L = 275 bar and V_L = 0.057 sm^3/t

2.2. Solution in formation water

As is known, normally natural gas cannot dissolve in water effectively, although under high pressure and temperature the volume which dissolves in water can reach significant amounts. Since the investigated reservoirs are under extreme conditions and the measured connate water saturation of the core samples was significant, it is clear that natural gas coming out from the solution must be taken into account. Solution depends on pressure, temperature, and salinity values. The solution is less effective if the salt content of the formation water is high. As natural gases mostly consist of methane, the calculation of methane solubility can provide adequate results. Blount and Price in 1982 developed two correlations for calculating the me-

thane solubility in formation water [6]. This work uses the correlation which provides a lower standard deviation value, *Equation (2).*

$$\log_e CH_4 = -1.4053 - 0.002332 \times T + 6.3 \times 10^{-6} \times T^2 - 0.004038 \times S - 7.579 \times 10^{-6} \times P + 0.5013 \times \log_e P + 3.235 \times 10^{-4} \times T \times \log_2 P \quad (2)$$

where standard deviation of residuals is 0.0706 and multiple R is 0.9943, T is the formation temperature [°F], P is the formation pressure [psi], and S is the formation salinity [grams/liter]. CH_4 is in standard cubic feet [sft^3] per petroleum barrel at 25 °C and atmospheric pressure. The validation of this correlation is 160 °F–464 °F (71 °C–240 °C) temperature and 3,500 psi–22,500 psi (241 bar–1,551 bar) pressure.

Methane solubility is greater with increasing pressure and temperature. Also, it is greater with decreasing salinity values, as is indicated by *Equation (2)*.

2.3. Derivation of pressure drop calculation

Material balance equations are one of the most powerful tools for a reservoir engineer to model the reservoir behavior and approximate the original gas in place. The main concept in generating the material balance equation is simply a volumetric balance, which states that the algebraic sum of volume changes of gas in reservoir and the gas produced must be zero. The reservoir temperature is assumed to be constant. In this study a material balance equation was necessary which deals with the fact of several different mechanisms. Because of the reservoir conditions a closed reservoir is assumed (in the case of tight, compact reservoir this assumption is acceptable) where the gas expansion, formation water expansion and formation rock expansion are the basic mechanisms. As a great deal of unconventional gas reservoirs are shale gas types, dealing with adsorption is indispensable. Because of the great pressures and temperatures the dissolution of natural gas in the connate formation water is necessary (also since the measured connate water saturation of the core samples was extremely high). Due to these phenomena the following connection is stated in this paper where the volumes are identified under reservoir conditions.

$$\begin{aligned} &Cumulative\ gas\ production\ [m^3] \\ &\quad = Gas\ expansion\ [m^3] + Rock\ and\ water\ expansion\ [m^3] + Desorption\ [m^3] \\ &\quad + Release\ from\ formation\ water\ [m^3] \end{aligned} \quad (3)$$

It is evident that due to the mechanisms taken into account the pressure depletion is not as high for all mechanisms as in the case of only a closed reservoir without desorption or release of natural gas from formation water. This statement is visualized in *Figure 2.*

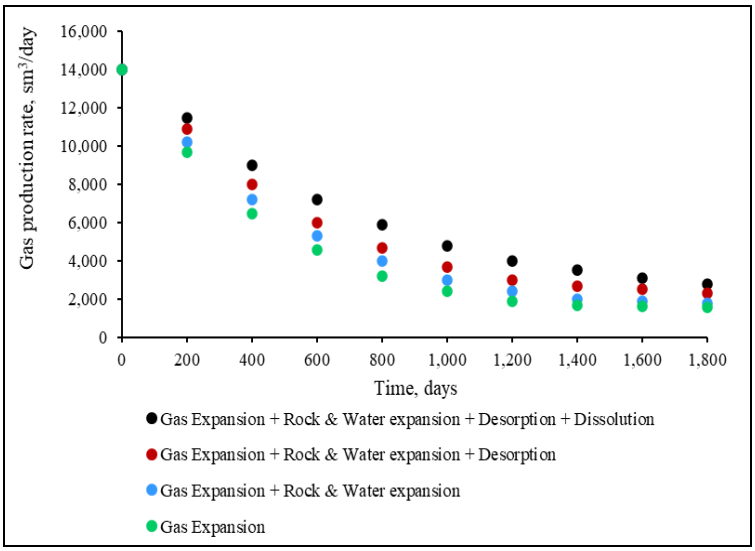

Figure 2
Behavoir of different material balances during production

Identification of the different parts of this connection can be seen in the following equations, where the Langmuir isotherm *(Equation 1)* was used for the desorbed gas volume calculation and *Equation (2)* was used for calculation of the release dissolved gas volume. Gas expansion and formation water and rock expansion calculation were calculated by clear equations.

$$Cumulative\ gas\ production\ [m^3] = G_p \times B_g \tag{4}$$

$$Gas\ expansion\ [m^3] = G_f \times (B_g - B_{gi}) = A \times h \times \Phi_{ci} \times (1 - S_{wi}) \times \left(\frac{B_g}{B_{gi}} - 1\right) \tag{5}$$

$$Rock\ and\ water\ expansion\ [m^3] = G_f \times B_{gi} \times \frac{S_{wi} \times c_w + c_f}{1 - S_{wi}} \times (p_i - p)$$
$$= A \times h \times \Phi_{ci} \times B_{gi} \times (S_{wi} \times c_w + c_f) * (p_i - p) \tag{6}$$

$$Desorption\ [m^3] = G_a \times \frac{1}{G_{ci}} \times B_g \times \left(\frac{V_L \times p_i}{P_L + p_i} - \frac{V_L \times p}{P_L + p}\right) = A \times h \times \rho_{bi} \times B_{gi} \times \left(\frac{V_L \times p_i}{P_L + p_i} - \frac{V_L \times p}{P_L + p}\right) \tag{7}$$

$$Release\ from\ formation\ water\ [m^3] = G_s \times B_g \times \frac{1}{V_{si}} \times \Delta V_s = A \times h \times \Phi_{ci} \times S_{wi} \times B_g \times \Delta V_s \tag{8}$$

Where the subscript $_i$ stands for values under initial reservoir conditions, G_p is the cumulative gas production under standard conditions [sm^3], G_f is the initial free gas volume under standard conditions [sm^3], G_a is the adsorbed gas volume under standard conditions [sm^3], G_s is the dissolved gas volume under standard conditions [sm^3], G_{ci} is the initial adsorbed gas content of the reservoir [sm^3/kg rock], V_{si}

is the initial dissolved gas content [sm^3/m^3], ΔV_s is the initial dissolved gas volume minus the dissolved gas volume under depleted reservoir pressure [sm^3/m^3], p_i is the initial pressure [Pa], A is the reservoir area [m^2], h is the reservoir height [m], B_{gi} is the initial formation volume factor [m^3/sm^3], B_g is the formation volume factor under depleted reservoir pressure [m^3/sm^3], Φ_{ci} is the corrected porosity [–], S_{wi} is the initial water saturation of the reservoir [–], V_L is the Langmuir volume [sm^3/kg], P_L is the Langmuir pressure [Pa], c_w is the water compressibility assumed to be equal to 45.8×10^{-11} [1/Pa], c_f is the formation compressibility [1/Pa] factor which can be calculated by Hall's correlation [7] who investigated 12 samples (7 limestones and 5 sandstones) to develop a c_f correlation, *Equation (9)*.

$$c_f = 1.86 \times 10^{-6} \times \Phi_m{}^{-0.415} \times \frac{1}{6{,}894.75729} \tag{9}$$

The use of corrected porosity is necessary because in this model the free gas volume is lower than when the adsorbed phase volume is ignored. The adsorbed gas is located on the surface of the pores, so it decreases the effective porosity. As the pressure decreases the adsorbed phase vaporizes (due to the Langmuir isotherm) and makes a vacant space that is instantly occupied by free gas. Thus, the pore volume available for free gas is allowed to increase as pore pressure decreases, in this case during production. Williams-Kovacs et al. [8] suggest a correction factor for this phenomenon presented in field unit, *Equation (10)*. It should be corrected with a Φ_{cm} term, suggested here, as the measured porosity (measured in laboratory conditions) is required in reservoir conditions, *Equation (11)*, suggested by Engler in 2010 [9].

$$\left(\frac{\Phi_{ac}}{\Phi_{cm}}\right) = \frac{\Phi_{cm} \times (1 - S_{wi}) - 1.318 \times 10^{-6} \times M \times \frac{\rho_b}{\rho_a} \times V_L \times \frac{p}{p + P_L}}{\Phi_{cm} \times (1 - S_{wi})} \tag{10}$$

$$\Phi_{cm} = \frac{e^{c_f \times (p_i - p_m)}}{\frac{1}{\Phi_m} - \left[1 - e^{c_f \times (p_i - p_m)}\right]} \tag{11}$$

where Φ_{ac} is the corrected porosity due to adsorbtion [–], Φ_{cm} is the corrected measured porosity [-], M is the gas molar mass [lb/lbmol], V_L is in [scf/t] and P_L is in psi, ρ_b/ρ_a is the reservoir bulk density over adsorbed phase density under initial conditions [–], where the adsorbed gas density is assumed to be equal to liquefied methane density, which is approximately 420 kg/m^3. Bulk density can be measured by laboratory circumstances (ρ_{bm}) and corrected by the formation compressibility under reservoir conditions, *Equation (12)*.

$$\rho_b = \rho_{bm} + \rho_{bm} \times c_f \times p_m \tag{12}$$

where p_m is the pressure during porosity measurement [Pa]. The initial corrected reservoir porosity is given by the following equation.

$$\Phi_{ci} = \Phi_{cm} \times \left(\frac{\Phi_{ac}}{\Phi_{cm}}\right) \tag{13}$$

Finally, the enhanced material balance equation suggested in this paper is presented below.

$$\begin{aligned} G_p \times B_g &= A \times h \times \Phi_{ci} \times (1 - S_{wi}) \times \left(\frac{B_g}{B_{gi}} - 1\right) + A \times h \times \Phi_{ci} \times B_{gi} \times (S_{wi} \times c_w + c_f) \times (p_i - p) \\ &+ A \times h \times \rho_{bi} \times B_g \times \left(\frac{V_L \times p_i}{P_L + p_i} - \frac{V_L \times p}{P_L \times p}\right) + A \times h \times \Phi_{ci} \times S_{wi} \times B_g \times \Delta V_s \end{aligned} \tag{14}$$

where B_g, B_{gi}, can be calculated by *Equation (15)* (in case of B_{gi} the equation is used by the initial deviation factor and with the initial reservoir pressure) and ΔV_s by the use of *Equation (2)* (where its value is equal to the volume under initial reservoir pressure minus the volume under depleted reservoir pressure).

$$B_g = \frac{P_{st} \times z \times T_i}{T_{st} \times p} \tag{15}$$

where P_{st} is the standard pressure (101,325 Pa), T_{st} is the standard temperature (298.15 K), z is the deviation factor of the gas under reservoir pressure [–]. The terms in ΔV_s are determined by SI units, so a C_1 correction factor is necessary to convert it back to psi and its value is 0.000145037738.

As pressure drop calculation is required to predict the gas production over several years this paper suggests a method based on the material balance equation presented above. *Equation (14)* is not a linear equation, so we suggested to solve the equation for depleted reservoir pressure (p) using Newton's method, which is an iterative calculation method. For this purpose, the function in *Equation (16)* is determined by rearrangement and simplification and the derivative of this function *(Equation 17)* is determined.

$$\begin{aligned} f(p) &= \frac{\beta 11}{p} + \beta 14 - \beta 3 \times p + \frac{\beta 13}{p} - \frac{\beta 4}{p} \times \frac{V_L \times p}{P_L \times p} + \frac{\beta 5}{p} \\ &\times \left[\beta 6 - e^{\beta 7 - \beta 8 \times (p \times C1) + \beta 9 \times \ln(p \times C1) + \beta 10 \times (p \times C1)}\right] - \frac{\beta 15}{p} \end{aligned} \tag{16}$$

$$\begin{aligned} f'(p) &= \frac{V_L \times \beta 4}{(p + P_L)^2} - \frac{\beta 5 \times \left(\frac{\beta 10}{p} + \frac{\beta 9}{p} - \beta 8 \times C1\right) \times e^{\beta 10 \times \ln(p \times C1) + \beta 9 \times \ln(p \times C1) - \beta 8 \times C1 \times p + \beta 7}}{p} \\ &- \frac{\beta 5 \times \left(\beta 6 - e^{\beta 10 \times \ln(p \times C1) + \beta 9 \times \ln(p \times C1) - \beta 8 \times C1 \times p + \beta 7}\right)}{p^2} + \frac{\beta 15}{p^2} - \frac{\beta 13}{p^2} - \frac{\beta 11}{p^2} - \beta 3 \end{aligned} \tag{17}$$

To find the solution a starting p_0 value should be chosen that is less than the initial formation pressure (assumed to be less by 1 bar). Then with *Equation (18)* the calculation of a new p value should be done. The procedure has to be continued until the difference between p_n and p_{n-1} is acceptably small.

$$p_n = p_{n-1} - \frac{f(p)}{f'(p)} \tag{18}$$

However, the deviation factor and the cumulative gas production also depend on the reservoir pressure (p). So after finding an acceptable p_n value the whole procedure should be recalculated with the recalculation of the deviation factor (z) and G_p (gas production rate calculations with different apparent permeability values – detailed in a later section) which now should be calculated with the new p_n pressure instead of the assumed p_0 pressure. So, the whole procedure is a double iteration method, as can be easily understood with the flow chart in *Figure 3.*

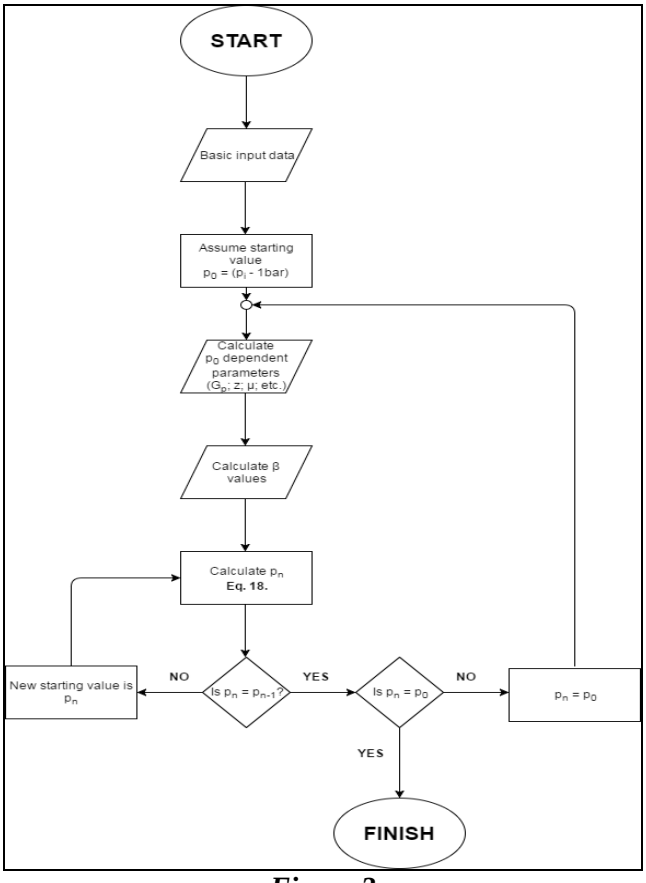

Figure 3

Algorithm flow chart for pressure drop calculation

The first step is to identify the constant values that are the basic input parameters during the calculations, including measured porosity, reservoir area, absolute permeability, reservoir height, Langmuir pressure and temperature, initial reservoir pressure and reservoir temperature, average pore radius, produced gas specific gravity, etc. Then if the calculation is the first iteration, we have to choose a starting depleted reservoir pressure where a 1 bar depletion from initial reservoir pressure is a good assumption in most cases. Otherwise, if the iteration is not the first one, we have to use the previously calculated depleted pressure (p_n). The next step is the calculation of the pressure dependent parameters (where the depleted pressure is necessary), such as the apparent permeability, gas deviation factor, and the cumulative gas production (where we have to identify the required time step). Then we need to calculate the initial values (corrected initial porosity, formation compressibility, initial reservoir bulk density etc.) and the β parameters that are necessary for *Equations (16)* and *(17).* Next the calculation of *Equation (18)* is necessary, where the starting pressure is the assumed depleted pressure (in the first iteration) or the depleted pressure determined in the previous iteration step. Then we have to determine if the resulted pressure is close enough to the starting pressure. If not, we must recalculate *Equation (18)* with the previously determined pressure (this iteration proceeds until two consecutive calculated pressures are close enough). If we get an acceptable value for depleted pressure, we need to determine if this pressure is close enough for the initial assumed (or previously determined pressure by the previous iteration process). If yes, we are finished with this process; if not, we have to attach back the calculated depleted pressure (after basic input data) and continue the whole process until we get a suitable depleted reservoir pressure.

The disadvantage of this method is the huge computational quantity, but it has a great advantage as most of the influential mechanisms are contained in the calculation. *Figure 2* shows how different material balances behave with different mechanisms accounted in them. The data used in them are listed in *Table 2*, except V_L is assumed to be equal to 10 sft^3/t and the reservoir is assumed horizontally fractured with 40 m fracture half-length and 10 stages, and the basic Darcy's model was used. The production rate does not drop as significantly in the case of material balance equation (MBE), which accounts for all of the detailed mechanisms as in case of other MBE (which take into account less mechanisms) because of the release of the dissolved natural gas in the connate water and desorbed gas during pressure depletion. All of the MBE can be reached with the presented model by neglecting the unnecessary terms, as can be seen in *Figure 2.*

3. GAS FLOW MODELS

The Darcy equation, which was derived from the Navier-Stokes equation based on continuum theory, has been used for more than 150 years to linearly relate fluid-flow rate and pressure gradient across a porous system. The linearity of the Darcy equation makes it easy and practical to use in reservoir engineering analysis and

numerical reservoir simulations. Darcy's equation correctly models the flow behavior at macrometrical and micrometrical scale where the main forces interacting are viscous. However, physics of fluid flow in shale and tight reservoirs cannot be predicted from standard flow or mass transfer models because of the presence of nanopores, ranging in size from one to hundreds of nanometers. Conventional continuum flow equations, such as Darcy's law, greatly underestimate the flow rate when applied to nanopore-bearing reservoirs [10].

This phenomenon can be described by the fact that with decreasing pore sizes the interacting forces between the pore walls and gas molecules are become significant than those between gas molecules (which is typical in viscous Darcy's flow). As this effect becomes more significant the flow will alter increasingly from the Darcy's flow. Also, when the pore sizes are small enough (comparable to molecule size) the main driving force becomes the concentration difference (diffusion) instead of the pressure difference.

To specify the magnitude of the alteration from Darcy type flow, different flow regimes are introduced. But before the characterization of the flow regimes, introduction of new expressions such as mean free path and Knudsen number are essential.

3.1. Mean free path

In a closed system, the molecules are constantly colliding with each other as they are not geometrical points. The average distance between the collisions is the mean free path [11]. A good visualization is given in *Figure 4*, where the molecule diameter is presented by d [m], so the collision area A [m^2] can be calculated by *Equation (19)*.

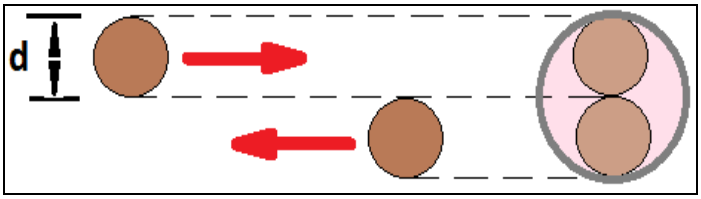

Figure 4. *Visualization of the mean free path*

$$A = d^2 \times \pi \tag{19}$$

In time the collision area will sweep out a cylindrical volume where n number of molecules is presented (treated as point masses). The molecules move with a constant speed along straight lines so the mean free path, λ [m] can be calculated as the length of the path divided by the number of collisions (volume of the cylinder, V [m^3] times the number of molecules per unit volume n), *Equation (20)*.

$$\lambda = \frac{l}{V \times n} = \frac{\bar{v} \times t}{\bar{v} \times t \times d^2 \times \pi \times n} = \frac{1}{d^2 \times \pi \times n} \tag{20}$$

The problem with this expression is that the average molecular velocity is used, but the target molecules are also moving, so the frequency of collisions depends upon the average relative velocity of the randomly moving molecules. The magnitude of the relative velocity is the square root of the scalar product of the velocity with itself *(Equation 21)*. The number of molecules per volume can be given by Avogadro's number, N_A (6.022×10^{23} mol^{-1}) and the ideal gas law. The ratio of the universal gas constant, R [8.314 J/(mol × K)] and Avogadro's number is the Boltzmann number, K_B (1.38×10^{-23} J/K). Finally, the corrected mean free path equation is given by *Equation (22)*.

$$\bar{v}_{rel} = \sqrt{2} \times \bar{v} \tag{21}$$

$$\lambda = \frac{R \times T}{\sqrt{2} \times d^2 \times \pi \times N_A \times p} = \frac{K_B \times T}{\sqrt{2} \times d^2 \times \pi \times p} \tag{22}$$

It is evident that the mean free path is proportional to pressure because at higher pressure, a greater amount of gas molecules can be present in a unit volume, so collisions between the molecules will be more common and decrease the value of the mean free path, *Figure 5*.

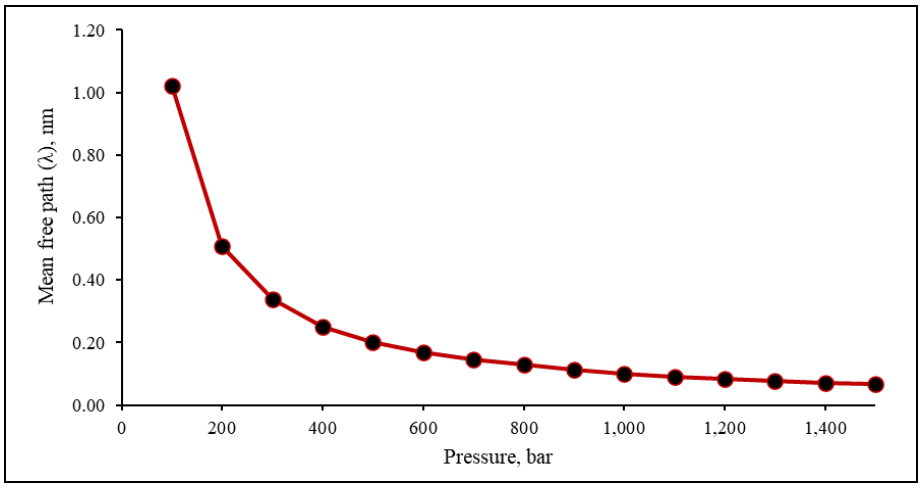

Figure 5

Mean free path vs. pressure diagram, using the investigated reservoir's data

3.2. Knudsen number

When the average mean free path of the gas molecules begins to be comparable or greater than the pore size containing it, the result is a break in the continuum theory. The degree of deviation from this theory is measured with the Knudsen number. The Knudsen number is calculated by the ratio of the mean free path and the pore

diameter ***(Equation 23)***. The value of this number is directly proportional to the mean free path, so as the average distance between the collisions of the molecules becomes smaller the Knudsen number decreases as well.

$$K_n = \frac{\lambda}{d} \tag{23}$$

If the pore diameter is much greater than the mean free path of the contained gas molecules, the value of Knudsen number is between 0 to 10^{-3} [–] and the flow behavior does not differ from the continuum flow [12]. When the mean free path is close to comparable to the pore diameter or exceeds it the flow becomes to alter from Darcy's flow and different types of flow regimes can be distinguished depending on the magnitude of the deviation. *Table 1* represents flow regimes corresponding to Knudsen number ranges [13].

Table 1

Types of different flow regimes as a function of Knudsen number [12]

Knudsen number [-]	Flow regime
$0–10^{-3}$	Continuum/Darcy flow (no-slip flow)
$10^{-3}–10^{-1}$	Slip flow
$10^{-1}–10^{1}$	Transitional flow
$10^{1}–\infty$	Free molecular flow/Knudsen diffusion

The different flow regimes are presented as a function of pressure in *Figure 6*, where different pore diameters are also investigated and the examined formation's properties presented in *Table 2* are shown as a red line.

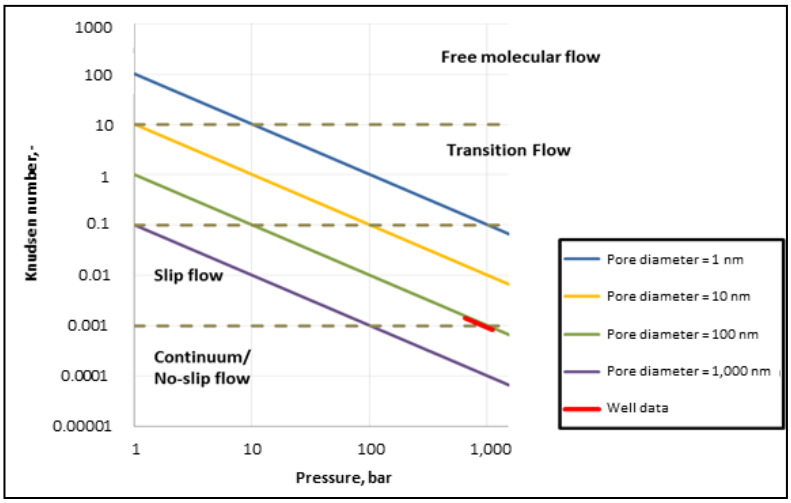

Figure 6

Representation of different flow regimes as a function of pressure and pore diameter

It can be observed that the flow regimes of the investigated formation are between the continuum flow and the slip flow regime. It is quite an interesting result, because as the investigated reservoir's properties are in extreme conditions, very non-continuum flow behavior can be presumed. This controversial observation can be explained by the fact that the value of Knudsen number is proportional to the pressure inversely, meaning that *Equation (24)* is not very accurate at high pressures. That is why it is predicting a mean free path smaller than the collision diameter at very high pressures [14].

3.3. Models

Different flow models investigated in this paper are collected and presented in *Figure 7*. All of them are expressed in an apparent permeability parameter divided by the absolute (or Darcy-constant) permeability. These apparent permeability values are functions of the pressure in all models. This is different than Darcy's model, where a constant value of permeability is determined. These models are expressed in different forms as their applicability is usually acceptable in one or two flow regimes. The derivations of the different models are not detailed in this paper nor the apparent permeability equations of them (the corresponding literature is listed in the references). Two types of flow regimes are investigated in this paper (in addition to the continuum regime). There are six types of models which deal with the slip flow regime and four types which deal with mainly the transitional regime. Also, a model which uses individual equations in case of different regimes is presented. It has to be mentioned that most of the models that account for Knudsen diffusion (typical mechanism in transitional regime besides slip phenomenon) are also suggested in the case of the slip regime, except for the NAP (non-empirical analytical permeability) model, which neglects the slip term and thus cannot describe appropriately the flow in this regime (see *Figure 7*). The models usually suggested to describe slip phenomenon are framed with green and models suggested in case of the transitional regime are framed with red. The following models were used (with references):

- Klinkenberg 1941 [15]
- Jones and Owens 1980 [16]
- Sampath and Keighin 1982 [17]
- Heid et al. 1950 [18]
- Florence et al. 2007 [19]
- Civan 2010 [20]
- Javadpour 2009 [10]
- Azom and Javadpour 2012 [21]
- APF – Darabi et al. 2012 [22]
- Sakhaee-Pour and Bryant 2012 [23]
- NAP – Singh et al. 2014 [24]

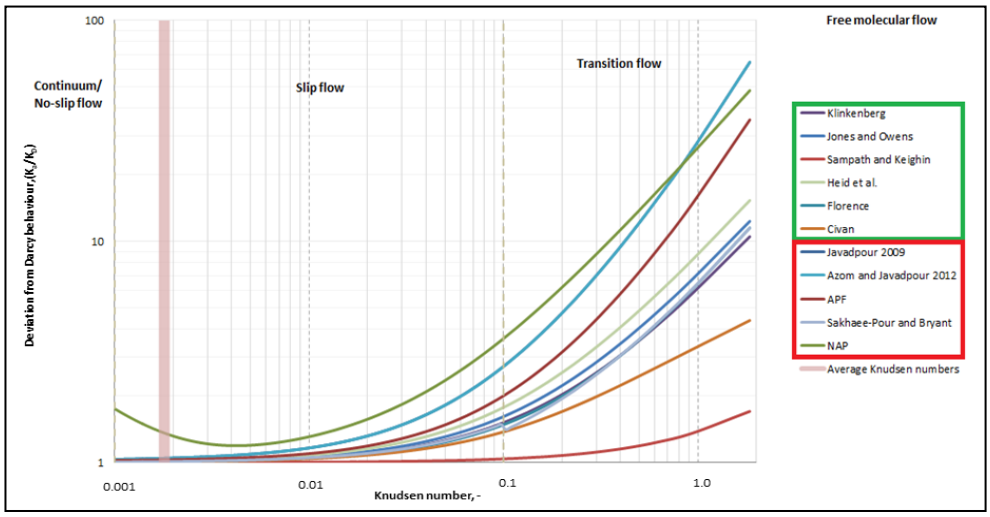

Figure 7. *Comparison of different flow models*

Also, the Knudsen range (different during production) of the investigated reservoir is marked with rose color. We can identify that the apparent permeability values constantly increase with increasing Knudsen number. These models do not underestimate the gas flow rate, as was earlier mentioned in the case of Darcy's flow. The models which account for Knudsen diffusion result in higher apparent permeability values, so higher gas flow rates are expected. These results are inline with the literature [25]. The investigated reservoir data are listed in *Table 2*. The investigated formation was at the depth 5,470–5,478.5 m and 43 core samples were taken along the whole interval, on which the measurements for most basic input data were performed. The Langmuir constants were assumed to be low based on corresponding literature [26].

Table 2

Investigated reservoir's parameters

Name	Symbol	Value	Unit
Absolute permeability	k_∞	0.0035	mD
Average porosity	Φ	2.29	%
Average pore radius	r_{av}	55.22	nm
Reservoir temperature	T	229	°C
Initial reservoir pressure	P_i	1,104.2	bar
Reservoir height	h	8.16	m
Wellbore radius	r_w	5.5	inch
Initial water saturation	S_{wi}	86.1	%
Flowing bottom hole pressure	P_{wf}	650	bar
Drainage radius	r_e	50	m
Langmuir volume	V_L	2	scf/tons
Langmuir pressure	P_L	4,000	psi
Bulk density	ρ_{bi}	2.63	g/cm^3
Average collision diameter	δ_{av}	0.39	nm

4. RESULTS

During production calculation this paper investigated a five-year period. Because of the very small permeability values no forecast was made of high production rates, which were proven by the calculations. The initial production rates and the cumulative gas productions for each model are presented in *Table 3*. Also, deviation from the Darcy permeability values is examined with percentages to the Darcy values. The pressure drop calculations were based on the algorithm presented earlier and open-hole production (radial flow) was assumed.

Table 3

Comparison of the different models' results in case of initial gas production rate and cumulative gas production for a 5-year period

Model	Initial production rate, m^3/day	Deviation from Darcy, %	Cumulative gas production, m^3	Deviation from Darcy, %
Darcy 1856	1,044.4	**0.00**	1,650,517	**0.00**
Klinkenberg 1941	1,048.9	**0.43**	1,657,087	**0.40**
Jones and Owen 1980	1,049.8	**0.51**	1,658,349	**0.47**
Sampath and Keighin 1982	1,044.8	**0.03**	1,651,003	**0.03**
Heid et al. 1950	1,051.2	**0.65**	1,658,349	**0.47**
Florence et al. 2007	1,048.1	**0.35**	1,655,882	**0.33**
Civan 2010	1,048.0	**0.34**	1,655,657	**0.31**
Javadpour 2009	1,063.8	**1.86**	1,677,526	**1.64**
Azom and Javadpour 2012	1,063.8	**1.85**	1,677,500	**1.63**
APF – Darabi et al. 2012	1,062.8	**1.76**	1,676,472	**1.57**
Sakhaee-Pour and Bryant 2012	1,048.8	**0.42**	1,656,902	**0.39**
NAP – Singh et al. 2014	1,994.6	**90.97**	2,714,736	**64.48**

The initial production rate values are so low that they make the formation impossible for economical production through an open-hole section. The necessity of enhanced gas recovery treatment is evident. However, the deviation from the Darcy production is higher in all cases (as was presumed by the models). The NAP, APF, Javadpour 2009 and Azom and Javadpour 2012 models provide higher production rates than the other models. This phenomenon can be elucidated by the fact that the reservoir is at the continuum–no-slip boundary *(Figure 7)* so the necessity of Knudsen flow is not required and the validity of these models during these conditions is questionable. Also, the NAP model yields very high production rates compared to other models, which can be accounted for by the fact that the model does not work properly in the Knudsen range of the reservoir. The other models provide very similar results for initial gas rate and cumulative gas production. As the flow type of the reservoir is very close to the continuum flow regime, it was expected that Darcy's flow calculations will result in almost acceptable production values. This assumption was proven by the calculations.

The reservoir pressure drop is not significant during the examined period because of the very low gas production rates. *Figure 8* shows the reservoir pressure

depletion and the cumulative gas production during the five-year period in the case of the Klinkenberg, 1941 model.

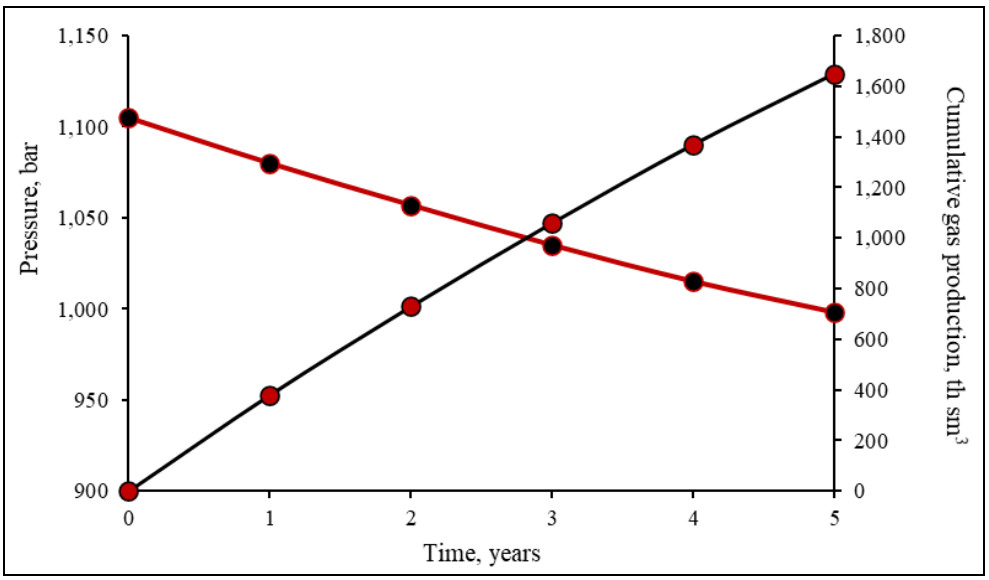

Figure 8
Pressure depletion and cumulative gas production for 5-year period with Klinkenberg, 1941 model

5. MODEL ADAPTABILITY FOR REAL PRODUCTION DATA

Results show that the calculation method suggested by this paper works well in case of the investigated reservoir but comparison of the results was not feasible because there were no available production data from the well. Therefore, another Hungarian natural gas well was built into the model to analyze the behavior of the model. The basic data of the investigated reservoir are shown in *Table 4*. As the reservoir is not a shale gas reservoir but a tight gas reservoir, the value of Langmuir pressure and Langmuir volume were chosen to be 0. There are three different productive zones in this formation and each of them was hydraulically fractured (vertical fracturing treatment). After test geophysical investigation and production tests it was determined that the three different fracture systems connect to each other and behave like one vertical fracture. Therefore, basic data were interpreted in this way. During test production 2,810,800 sm^3 natural gas and negligible amounts of condensate and water were produced. The initial gas production rate was about 36,000 sm^3/day, which coincides with the results forecast by the model suggested in this paper. The basic data and the production data were provided by company MOL Nyrt.

Table 4

Basic parameters of the investigated reservoir

Name	Symbol	Value	Unit
Absolute permeability	k_{∞}	0.008	mD
Average porosity	Φ	8.22	%
Reservoir temperature	T	473.15	K
Initial reservoir pressure	P_i	561	bar
Reservoir height	h	180	m
Area of the reservoir	A	0.02	km^2
Wellbore radius	r_w	0.14	inch
Initial water saturation	S_{wi}	55.4	%
Flowing bottom hole pressure	P_{wf}	266	bar
Fracture half length	x_f	50	m
Length of the flow	L	130	m

The investigated reservoir was in the continuum–slip boundary as well so the simple Darcy's model and the Civan, 2010 model (slip model) was interpolated on the production data, *Figure 9*. As can be seen, there is no excessive deviation between the two models. The interpolated graph fitted acceptably on the measured values, so the model suggested by this paper, works in a practicable range.

Although in case of reservoirs where flow regimes are in different than continuum regime can be calculated by different models

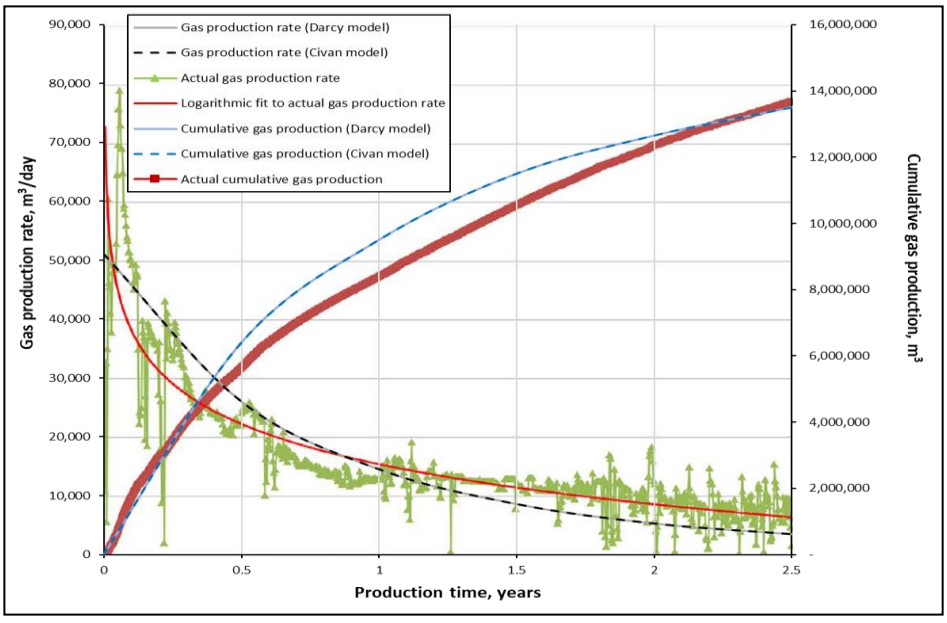

Figure 9

Plotting calculated data to real well data [27]

6. CONCLUSION

This paper described different types of unconventional gas reservoirs and described the different flows which come into prominence due to micro- and nanopore regimes. A Hungarian formation was characterized through the introduced flow equations and a new material balance equation. The material balance, which involves the detailed role of adsorbed gas in the porous matrix, provides reliable calculation of pressure depletion during production and original gas in place.

The performed measurements on the core samples provide the basic input parameters in the calculations. The reservoir is under extreme conditions, so different models had to be evaluated to gain a broader understanding of the reservoir behavior. As the reservoir is in the slip flow regime the most reliable data are assumed to be provided by the slip flow models.

The reservoir production was investigated in a five-year period by the presented calculation algorithm using all models. As no production data were available from the well, gas production data of another Hungarian well were used to investigate the application and adaptability of the model. The results proved the model works in a practicable range.

ACKNOWLEDGMENTS

The research was carried out in the framework of the GINOP-2.3.2-15-2016-00010 *Development of enhanced engineering methods with the aim at utilization of subterranean energy resources* project of the Research Institute of Applied Earth Sciences of the University of Miskolc in the framework of the Széchenyi 2020 Plan, funded by the European Union, co-financed by the European Structural and Investment Funds.

REFERENCES

[1] Haghshenas, B., Clarkson C. R., Chen, S. (2014). *New Models for Reserve Estimation and Non-Darcy Gas Flow in Shale Gas Reservoirs*. Paper presented at the SPE/EAGE European Unconventional Resources Conference and Exhibition, Vienna, Austria, SPE-167789-MS. https://doi.org/10.2118/167789-MS.

[2] Clarkson, C. R., Haghshenas, B. (2013). *Modeling of Supercritical Fluid Adsorption on Organic-Rich Shales and Coal*. Paper presented at the SPE Unconventional Resources Conference-USA, The Woodlands, Texas, USA, SPE-164532-MS, https://doi.org/10.2118/164532-MS.

[3] Wang, F. P., Reed, R. M. (2009). *Pore Network and Fluid Flow in Gas Shales*. Paper presented at the SPE Annual Technical Conference and Exhibition, New Orleans, Louisiana, SPE-124253-MS. https://doi.org/10.2118/124253-MS.

[4] Pápay, J. (2013). *Exploitation of Unconventional Petroleum Accumulations*. Akadémiai Kiadó, Budapest.

[5] Langmuir, I. (1918). The adsorption of gases on plane surfaces of glass, mica and platinum. *Journal of American Chemical Society*, 40 (9), pp. 1361–1403, https://doi.org/10.1021/ja02242a004.

[6] Blount, C. W., Price, L. C. (1982). *Solubility of methane in water under natural conditions: a laboratory study*. Final Report, Idaho State University, Pocatello (USA), Department of Geology, https://doi.org/10.2172/5281520.

[7] Hall, H. N. (1953). Compressibility of Reservoir Rocks. *Journal of Petroleum Technology*, 5 (1), pp. 17–19, SPE-953309-G. https://doi.org/10.2118/953309-G.

[8] Williams-Kovacs, J., Clarkson, C., Nobakht M. (2012). Impact of Material Balance Equation Selection on Rate-Transient Analysis of Shale Gas. *Paper presented at the SPE Annual Technical Conference and Exhibition*, San Antonio, Texas, USA, SPE-158041-MS, https://doi.org/10.2118/158041-MS.

[9] Engler, T. W. (2010). *Multiphase Phenomena—Fluid Flow in Porous Media*. Chapter 5. New Mexico Institute of Mining and Technology, Socorro, New Mexico, pp. 1–55.

[10] Javadpour, F. (2009). Nanopores and Apparent Permeability of Gas Flow in Mudrocks (Shales and Siltstone). *Journal of Canadian Petroleum Technology*, 48 (8), pp. 16–21, https://doi.org/10.2118/09-08-16-DA.

[11] Knight, R. D. (2004). *Physics for Scientists and Engineers: A Strategic Approach*. Pearson/Addison Wesley, San Francisco.

[12] Cussler, E. L. (2009). *Diffusion: Mass Transfer in Fluid Systems*. Cambridge University Press, Cambridge.

[13] Rezaee, R. (2015). *Fundamentals of Gas Shale Reservoirs*. John Wiley & Sons, Inc., Hoboken, NJ, https://doi.org/10.1002/9781119039228.

[14] Javadpour, F., D. Fisher, D., Unsworth, M. (2007). Nanoscale gas flow in shale gas sediments, *Journal of Canadian Petroleum Technology*, 46 (10). https://doi.org/10.2118/07-10-06.

[15] Klinkenberg, L. J. (1941). The Permeability of Porous Media to Liquids and Gases, Paper presented at the Drilling and Production Practice, New York, API-41-200.

[16] Jones, F. O., Owens, W. W. (1980). A Laboratory Study of Low-Permeability Gas Sands. *Journal of Petroleum Technology*, 32 (9), pp. 1631–1640, SPE-7551-PA, https://doi.org/10.2118/7551-PA.

[17] Sampath, K., Keighin, W. C. (1982). Factors Affecting Gas Slippage in Tight Sandstones of Cretaceous Age in the Uinta Basin. *Journal of Petroleum Technology*, 34 (11), pp. 2715–2720, SPE-9872-PA. https://doi.org/10.2118/9872-PA.

[18] Heid, J. G., McMahon, J. J., Nielsen, R. F., Yuster, S. T. (1950). *Study of the permeability of rocks to homogeneous fluids*. Paper presented at the Drilling and Production Practice, New York, API-50-230.

[19] Florence, F. A., Rushing, J., Newsham, K. E., Blasingame T. A. (2007). *Improved Permeability Prediction Relations for Low Permeability Sands*. Paper presented at the Rocky Mountain Oil & Gas Technology Symposium, Denver, Colorado, U.S.A., SPE-107954-MS, https://doi.org/10.2118/107954-MS.

[20] Civan, F. (2010). Effective Correlation of Apparent Gas Permeability in Tight Porous Media. *Transport in Porous Media*, 82, pp. 375–384. https://doi.org/10.1007/s11242-009-9432-z.

[21] Azom, P., Javadpour, F. (2012). *Dual-continuum modeling of shale and tight gas reservoirs*. Paper presented at the SPE annual technical conference and exhibition, San Antonio, Texas, SPE-159584-MS. https://doi.org/10.2118/159584-MS.

[22] Darabi, H., Ettehad, A., Javadpour, F., Sepehrnoori, K. (2012). Gas flow in ultra-tight shale strata. *Journal of Fluid Mechanics*, 710, pp. 641–658. https://doi.org/10.1017/JFM.2012.424.

[23] Sakhaee-Pour, A., Bryant, S. L. (2012). *Gas Permeability of Shale, The University of Texas at Austin*. Paper presented at the SPE Annual Technical Conference and Exhibition, Denver, Colorado, USA, SPE-146944-MS. https://doi.org/10.2118/146944-MS.

[24] Singh, H., Javadpour, F., Ettehadtavakkol, A., Darabi, H. (2014). Nonempirical apparent permeability of shale. *SPE Reservoir Evaluation & Engineering*, 17 (3), pp. 414–424, SPE-170243-PA, https://doi.org/10.2118/170243-PA.

[25] Singh, H., Javadpour, F., Ettehadtavakkol, A., Darabi, H. (2014). Nonempirical apparent permeability of shale. *SPE Reservoir Evaluation & Engineering*, 17 (3), pp. 414–424, SPE-170243-PA, https://doi.org/10.2118/170243-PA.

[26] Badics B., Uhrin A., Vető I., Bartha A., Sajgó Cs. (2011). Medenceközponti földgáz-előfordulás elemzése a Makói-árokban. Hungarian Geological Society, *Földtani Közlöny*, 141 (1), pp. 23–40.

[27] Kiss K. (2014). *Magyarországi repesztések tapasztalatai, üzenetei*. Presentation material, Budapest, 30. 10. 2014, Access date: 10. 10. 2021, Access: http://docplayer.hu/19983811-Magyarorszagi-repesztesek-tapasztalatai-uzenete-kiss-karoly-kutatasi-projektek-vezeto-2014-10-30-budapest.html.